#### **ELECTRON MICROSCOPY**

# Identification of site-specific isotopic labels by vibrational spectroscopy in the electron microscope

Jordan A. Hachtel<sup>1\*</sup>, Jingsong Huang<sup>1,2</sup>, Ilja Popovs<sup>3</sup>, Santa Jansone-Popova<sup>3</sup>, Jong K. Keum<sup>1,4</sup>, Jacek Jakowski<sup>1,2</sup>, Tracy C. Lovejoy<sup>5</sup>, Niklas Dellby<sup>5</sup>, Ondrej L. Krivanek<sup>5</sup>, Juan Carlos Idrobo<sup>1\*</sup>

The identification of isotopic labels by conventional macroscopic techniques lacks spatial resolution and requires relatively large quantities of material for measurements. We recorded the vibrational spectra of an  $\alpha$  amino acid, L-alanine, with damage-free "aloof" electron energy-loss spectroscopy in a scanning transmission electron microscope to directly resolve carbon-site–specific isotopic labels in real space with nanoscale spatial resolution. An isotopic red shift of 4.8  $\pm$  0.4 milli–electron volts in C–O asymmetric stretching modes was observed for  $^{13}\text{C}$ -labeled L-alanine at the carboxylate carbon site, which was confirmed by macroscopic infrared spectroscopy and theoretical calculations. The accurate measurement of this shift opens the door to nondestructive, site-specific, spatially resolved identification of isotopically labeled molecules with the electron microscope.

sotopic labeling of molecules is a widely employed technique for isolating chemical effects in complex biological experiments (1). The detection of isotopic labels is most frequently accomplished with mass spectrometry, but the resulting sample destruction can lead to the loss of valuable structural information. Alternatively, isotopes can be resolved through shifts in the vibrational modes corresponding to the changes in atomic mass, allowing techniques such as infrared and Raman spectroscopy or inelastic neutron scattering to identify isotopic labels and biomarkers to observe dynamic changes in molecular chemistry (2–6).

However, these macroscopic techniques lack spatial resolution and require relatively large quantities of sample for accurate measurement. To improve sensitivity to local heterogeneities. researchers have used tip-enhanced Raman spectroscopy (TERS) and scanning near-field optical microscopy (SNOM) to examine the vibrational spectra of biomolecules with high spatial and spectral resolution (7, 8). Electron microscopy has also shown promise for life science applications, especially in cryogenic experiments (9, 10), and provides spatially resolved access to a set of samples and experiments complementary to those of TERS and SNOM. Recently, breakthroughs in electron monochromation have allowed electron energy-loss spectroscopy (EELS) to access vibrational modes in solids with high spatial where the probe interacts with the sample without directly irradiating the material, allowing for efficient, damage-free vibrational spectroscopy of organic molecules outside of cryogenic conditions (17-21). We present here the spatial and spectral identification of site-specific isotopic labels in an amino acid obtained in a scanning transmission electron microscope (STEM). We used aloof monochromated EELS in an aberration-corrected STEM to examine L-alanine (L-Ala) and its <sup>13</sup>Clabeled counterpart. An isotopic shift of 4.8  $\pm$ 0.4 meV was measured with EELS, which is consistent with Fourier transform infrared (FTIR) spectroscopy experiments. Additionally, we used density functional theory (DFT) calculations to

resolution (11-14). Previous isotopic analysis in

the electron microscope had been conducted

through measurement of knock-on damage and

Compton scattering (15, 16) but required high

electron doses that are incompatible with beam-

sensitive materials. Vibrational EELS, on the

other hand, can be performed in "aloof" mode,

between <sup>12</sup>C and <sup>13</sup>C L-Ala with nanoscale precision. The samples were prepared by crushing and dispersing the high-purity crystalline powders onto TEM grids (crystal structure shown schematically in fig. S1). For the <sup>13</sup>C-labeled L-Ala particles, we used powders enriched at the carboxylate site. Small clusters of L-Ala (sizes varying from hundreds of nanometers to tens of micrometers) were then accessible on the lacy carbon support membrane. The L-Ala clusters were much thicker than the membrane and thus dominated the EEL spectrum. In this study, the spectra were taken from larger particles, with micrometer-scale di-

mensions to maximize signal-to-noise ratio, but

demonstrate that the isotopic shifts observed in

the  $^{12}\mathrm{C}$  and  $^{13}\mathrm{C}$  L-Ala samples primarily originate

from the carboxylate group. By using the highly

localized electron probe, we spatially distinguished

the spectra can also be acquired from the smaller hundred-nanometer-scale particles, as shown in the supplementary materials (fig. S2).

The aloof EEL spectra of <sup>12</sup>C and <sup>13</sup>C-labeled L-Ala (Fig. 1A) show a strong overlap between the majority of the peaks but with substantial differences in the highest intensity features in these spectra. To validate and expand on the EELS vibrational results, we obtained FTIR spectra from samples prepared using the same materials. The FTIR and EELS measurements have energy resolutions of 1 and 6 meV, respectively, hence the FTIR spectra were convolved with a 6-meV full width at half maximum (FWHM) Gaussian to match the energy resolution in EELS (Fig. 1B). The FTIR spectra in their as-acquired resolution are also shown for comparison (Fig. 1C). A comparison of the entire FTIR and EEL vibrational spectra of L-Ala is shown in the supplementary materials (fig. S3).

The EEL and FTIR spectra, for both the <sup>12</sup>C and <sup>13</sup>C samples, exhibited a dominant peak at  $\sim$ 200 meV (1600 cm<sup>-1</sup>). The  $\sim$ 200-meV peak was red-shifted in both techniques by the isotopic labels, whereas the majority of the other features in the <sup>12</sup>C spectrum were almost unchanged in the <sup>13</sup>C spectrum. The shift in the dominant peak of the EEL spectrum was measured statistically to be  $4.8 \pm 0.4$  meV (see below). In the FTIR experiment, the shift was measured from the maximum intensities of the dominant peaks in each isotopic sample at the as-acquired resolution, resulting in a shift of 4.9 meV. The presence of a consistent large shift of the dominant spectral feature allows for unambiguous differentiation between the two isotopic species with vibrational EELS.

Additionally, there was a 2.2% energy offset observed in the ~200-meV peak between FTIR and EEL spectra for both isotopic species. The cause of the offset could arise from the fact that EELS interacts mostly with the surface, whereas FTIR spectroscopy interacts with the entire cluster, because surface effects can alter the detected frequency of a vibrational mode (22). Alternatively, the offset could stem from subtle differences in the way that the selection rules affect vibrational fine structure for electron and photon excitations. We examined the correlation between spectral features in EELS and FTIR spectroscopy in greater detail (fig. S4) and found that all of the other EELS peaks had energies within 1% of the corresponding FTIR peaks. The match of the other spectral features indicates that the offset is a genuine difference in the detected peak positions of the same feature in the two spectroscopy techniques.

DFT calculations were performed for the fundamental vibrations of L-Ala with and without isotope substitutions to help assign vibrational modes to the experimentally observed peaks in EEL and FTIR spectra. Prior to the calculations, x-ray diffraction (XRD) analysis was performed on the purchased L-Ala sample, which showed that the powder is crystalline with a standard orthorhombic structure (fig. S5). The lattice parameters are in good agreement with previously

 <sup>&</sup>lt;sup>1</sup>Center for Nanophase Materials Sciences, Oak Ridge National Laboratory, Oak Ridge, TN 37831, USA.
 <sup>2</sup>Computational Sciences and Engineering Division, Oak Ridge National Laboratory, Oak Ridge, TN 37831, USA.
 <sup>3</sup>Chemical Sciences Division, Oak Ridge National Laboratory, Oak Ridge, TN 37831, USA.
 <sup>4</sup>Neutron Scattering Division, Oak Ridge National Laboratory, Oak Ridge, TN 37831, USA.
 <sup>5</sup>Nion R&D, Kirkland, WA 98034, USA.

<sup>\*</sup>Corresponding author. Email: hachtelja@ornl.gov (J.A.H.); idrobojc@ornl.gov (J.C.I.)

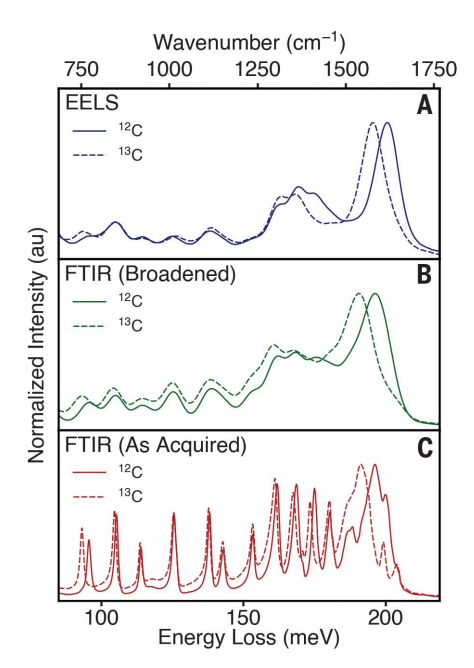


Fig. 1. Isotopic sensitivity in vibrational EELS (A) Experimental vibrational spectra acquired with monochromated aloof EELS for 12C L-Ala (solid line) and <sup>13</sup>C-labeled L-Ala (dashed line), exhibiting an observable isotopic shift of the dominant peak. (B) FTIR vibrational spectra from the same powders used for the EEL spectra in (A), broadened with a Gaussian filter to match the energy resolution in EELS (~6 meV) and showing a highly similar shift of the dominant peak. (C) FTIR spectra in the as-acquired energy resolution. Au, arbitrary units.

reported values (23, 24) and indicate that the L-Ala molecules exist in zwitterionic form in the powder. A supercell model of 35 zwitterionic L-Ala molecules was then constructed on the basis of the atomic coordinates from experimental measurements. Within this supercell model, an inner layer of nine molecules was geometrically optimized and used to produce the vibrational spectra, and the outer layer of 26 molecules was used to enforce the L-Ala crystalline environment and lock the molecules in their zwitterionic form (fig. S1). The calculations returned the energy, intensity, and atomic displacement vectors of the vibrational eigenmodes of crystalline L-Ala, which were then broadened with a 6-meV FWHM Gaussian to match the EELS energy resolution.

Figure 2 shows the vibrational eigenvalues and spectrum of the L-Ala supercell with the carbon atoms as their naturally occurring <sup>12</sup>C isotope (top panel). The eigenvalues (black vertical lines) reveal many vibrational modes spread throughout the IR range that merge together to form individual peaks in the Gaussian-convolved spectrum. A one-to-one correspondence is observed between the main peak groups in FTIR and DFT spectra. Some small differences are observed in peak intensity and frequency between experiment and theory, which is discussed in greater detail in the supplementary materials (fig. S6).

The DFT peak groups can be used to assign eigenmodes and displacement vectors directly to the experimental peaks. The dominant ~200-meV peak is seen to be mainly the C-O asymmetric stretching modes in the COO<sup>-</sup> group. The other strong peaks are bending modes in the NH<sub>3</sub><sup>+</sup> group at ~190 meV and coupled vibrations between C-C stretching and various symmetric and asymmetric deformations in CH3 and COOgroups for three subpeaks between 160 and 180 meV. The remaining smaller peaks are mostly bending deformation modes in the CH3 and NH<sub>3</sub><sup>+</sup> groups. The assignment of these vibrational modes is in good agreement with other calculations of the L-Ala zwitterion (25).

To examine the influence of isotopes, the vibrational response was recalculated upon 13C labeling of each carbon site in the molecule: the  $\alpha$  site bonded to the NH<sub>3</sub><sup>+</sup> group, the  $\beta$  site on the methyl side chain, and the carboxylate, or C'. site, which are shown below the all-12C calculation in Fig. 2. For the  $\alpha$  and  $\beta$  sites, only changes to weak oscillators are observed, which are washed out in the Gaussian-broadened spectra. However, <sup>13</sup>C labeling in the carboxylate site resulted in a substantial red shift for the main C-O asymmetric stretching mode, clearly observed in the broadened spectrum, that corresponds to the shifted ~200-meV peak in the EELS and FTIR measurements. Experimental differences between the C' enrichment and the  $\alpha$ - and  $\beta$ -site enrichment are shown in FTIR measurements in fig. S7. These differences show that the sensitivity of vibrational spectroscopy is connected to the oscillator strengths of the different modes along with the magnitude of the shift.

The magnitude of the shift induced by the heavier <sup>13</sup>C atom in the carboxylate site is closely related to the change in the reduced mass of a C-O pair  $(\sqrt{\mu^{13}CO/\mu^{12}CO})$ : a shift factor of ~1.022. The shift factors from the experiments yielded similar values: 1.026 for both FTIR spectroscopy and EELS. The DFT calculations predicted a larger-magnitude shift in the C-O stretching modes, 6.5 meV compared with ~5 meV, but this value corresponds to a shift factor of 1.033, which is within 1% of the experimental values. The agreement corroborates our understanding that the dominant peak in the EEL and FTIR spectra is from the C-O stretching vibrational modes, and that vibrational EELS can distinguish between isotopic labels at specific sites in organic molecules.

To precisely measure the isotopic shift in EELS and to quantify the precision of the measurement, we acquired a series of 100 EEL spectra from each L-Ala sample. Figure 3A shows individual low signal-to-noise ratio (SNR) EEL spectra from <sup>12</sup>C and <sup>13</sup>C L-Ala sequences, respectively, with the corresponding Lorentzian fits to the C-O peak. The distribution and average of the fitted peak centers are plotted in Fig. 3B. The C-O peak was measured to be at 200.5 meV for the <sup>12</sup>C L-Ala and at 195.7 meV for <sup>13</sup>C L-Ala (a shift of 4.8 meV), with standard deviations of 0.2 meV

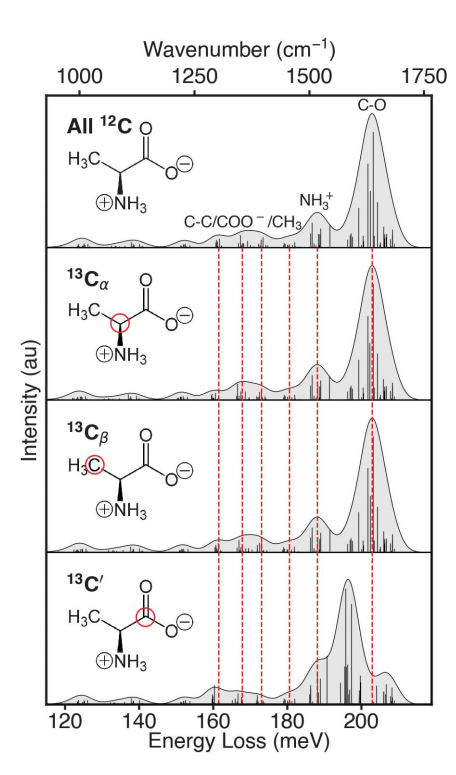
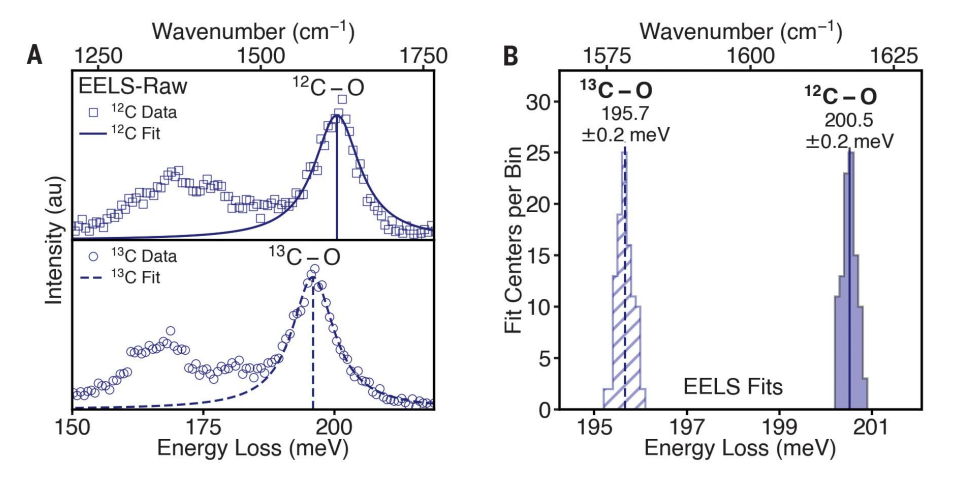


Fig. 2. Influence of isotopic enrichment at specific carbon sites. DFT-calculated vibrational eigenvalues (black vertical lines) and corresponding Gaussian-broadened spectra for L-Ala with its naturally occurring <sup>12</sup>C isotope and with <sup>13</sup>C isotopic labeling at each of the three carbon sites— $C_{\alpha}$  site,  $C_{\beta}$  site, and C' site (shown schematically in the insets by red circles)—demonstrating a large shift from C'-site labeling. The red dashed vertical lines indicate the centers of the main peak groups observed in the calculated <sup>12</sup>C L-Ala spectrum.

for each series of measurements. The magnitude of the error is just 0.2 meV, which is less than 5% of the total isotopic shift, demonstrating highprecision isotopic identification.

Finally, we dispersed both 12C and 13C L-Ala clusters on the same sample grid. Figure 4A shows a STEM dark-field image of a region extending between two L-Ala clusters (12C on the left, <sup>13</sup>C on the right). We took an EELS line profile across this region, acquiring a sequence of 75 spectra at each probe position, and fit Lorentzians to the C-O stretching peak for each individual spectrum. The corresponding fits of the summed data (Fig. 4B) show that the EEL intensity was centered on the 12C-O frequency when the probe was near the left cluster, and on the 13C-O frequency when the probe was near the right cluster. The C-O stretching mode was detected as a mix of the two in the vacuum between the two clusters, providing a real-space picture of the isotopic shift between the <sup>12</sup>C and C L-Ala clusters.

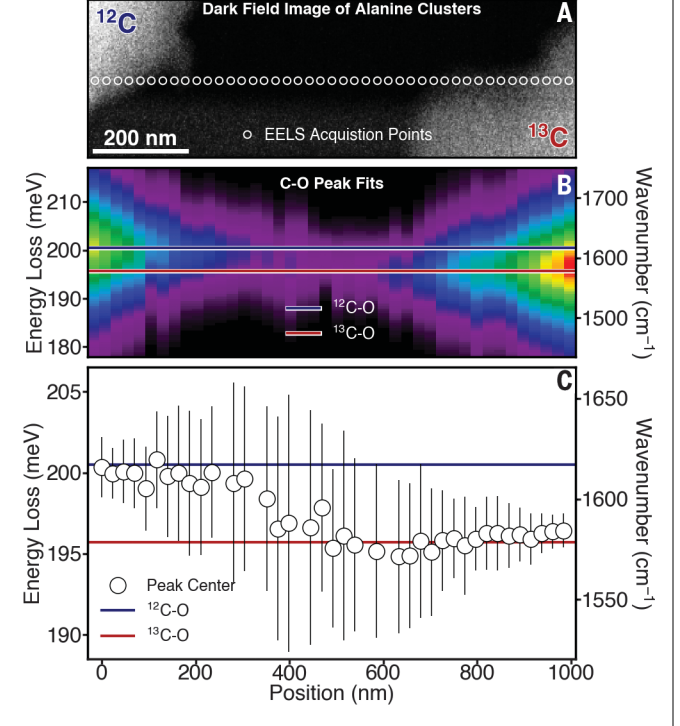
The C-O peak intensity was highly localized to the L-Ala clusters. The summed peak center and standard deviation of each 75-spectrum



**Fig. 3. Precision of isotopic sensitivity.** (**A**) Raw EEL spectrum acquired from <sup>12</sup>C and <sup>13</sup>C L-Ala samples, with a Lorentzian fit of the C–O peak. To perform high-precision measurements, 100 spectra were acquired and fitted. (**B**) Histogram of fitted peak positions from all acquisitions in both samples, demonstrating a 4.8-meV peak shift with <1-meV precision.

## Fig. 4. High-spatial resolution isotopic analysis.

(A) Dark-field image of <sup>12</sup>C (left) and <sup>13</sup>C (right) ∟-Ala clusters. EELS was acquired along a line profile between the two clusters (circles). (B) Lorentzian fits of the magnitude and position of the C-O EELS peak, plotted for each point shown in the line profile in (A). (C) Peak center and standard deviation for the Lorentzian fits shown in (B), demonstrating the high-spatial resolution identification of isotopic species.



sequence along the line profile is plotted in Fig. 4C. The error bars here, determined by the standard deviation of the individual fits, show that the C-O shift could be reliably obtained from individual noisy spectra while close to the clusters, but for large impact parameters, the peak fit requires the summed data. For several probe positions, the fitting routine returned unphysical results and these five data points were removed as outliers (fig. S8).

The particles here were separated by several hundred nanometers, which is an order of magnitude below the optical diffraction limit (~3.1  $\mu$ m for excitations at an energy of 200 meV), and the true spatial resolution of the technique is much

higher. A line scan on a single L-Ala cluster showed that the intensity of the signature C-O peak fell off sharply as a function of the distance from the cluster. The vibrational EEL spectra from the line scan are presented in the supplementary materials (fig. S9) and show that the intensity is reduced by 20% after 25 nm and by 50% after 100 nm. Additionally, by calculating the delocalization of inelastic scattering, we can estimate the sample depth from which the majority of the signal originates. For a primary beam energy of 30 keV, at an energy loss of 200 meV and an impact parameter of 5 nm, this value is estimated to be ~50 nm (more details in the supplementary materials). The two estimates

of the maximum vibrational spatial resolution indicate that clusters much closer together could still be resolved using EELS.

The capacity to produce high-SNR, high-energy resolution spectra from minute quantities of organic material makes vibrational EELS a strong complement to conventional techniques. Further progress in this rapidly advancing technique and experiments involving larger isotopic differences should enable nanoscale versions of traditionally macroscopic experiments, such as isotopic concentration measurements and, potentially, carbon dating. Additionally, one can perform direct vibrational mapping of beam-sensitive samples by using "leap-frog" scanning, where the electron probe is advanced in discrete steps and blanked between acquisitions. The area directly irradiated by the beam is destroyed, but the surrounding area is undamaged and probed by the aloof EELS (26). When combined with cryogenic sample preparation, isotope-labeled proteins could be tracked in real space in whole-cell samples with the resolution of the electron microscope, resulting in direct observation of intracellular molecular chemistry.

#### **REFERENCES AND NOTES**

- S. Radajewski, I. R. McDonald, J. C. Murrell, *Curr. Opin. Biotechnol.* **14**, 296–302 (2003).
- 2. A. Barth, Prog. Biophys. Mol. Biol. 74, 141-173 (2000).
- 3. M. J. Albers et al., Cancer Res. 68, 8607-8615 (2008).
- S.-H. Shim et al., Proc. Natl. Acad. Sci. U.S.A. 106, 6614–6619 (2009).
- G. J. Kearley, M. R. Johnson, Vib. Spectrosc. 53, 54–59 (2010).
- R. Adhikary, J. Zimmermann, F. E. Romesberg, Chem. Rev. 117, 1927–1969 (2017).
- 7. I. Amenabar et al., Nat. Commun. 4, 2890 (2013).
- R. L. Agapov, J. D. Scherger, A. P. Sokolov, M. D. Foster, J. Raman Spectrosc. 46, 447–450 (2015).
- M. A. Aronova, R. D. Leapman, MRS Bull. 37, 53–62 (2012).
- 10. D. Sirohi et al., Science 352, 467-470 (2016).
- 11. O. L. Krivanek et al., Nature 514, 209-212 (2014).
- 12. C. Dwyer et al., Phys. Rev. Lett. 117, 256101 (2016).
- M. J. Lagos, A. Trügler, U. Hohenester, P. E. Batson, *Nature* 543, 529–532 (2017).
- 14. F. S. Hage et al., Sci. Adv. 4, eaar7495 (2018).
- 15. T. Susi et al., Nat. Commun. 7, 13040 (2016).
- G. Argentero, C. Mangler, J. Kotakoski, F. R. Eder, J. C. Meyer, Ultramicroscopy 151, 23–30 (2015).
- 17. P. Rez et al., Nat. Commun. 7, 10945 (2016)
- 18. P. A. Crozier, *Ultramicroscopy* **180**, 104–114 (2017).
- 19. J. C. Idrobo et al., Phys. Rev. Lett. 120, 095901 (2018).
- D. M. Haiber, P. A. Crozier, ACS Nano 12, 5463–5472 (2018).
- 21. J. R. Jokisaari et al., Adv. Mater. 30, 1802702 (2018).
- 22. A. A. Govyadinov et al., Nat. Commun. **8**, 95 (2017).
- 23. N. P. Funnell et al., CrystEngComm 12, 2573–2583 (2010).
- 24. M. S. Lehmann, T. F. Koetzle, W. C. Hamilton, *J. Am. Chem. Soc.* **94**, 2657–2660 (1972).
- E. Tajkhorshid, K. J. Jalkanen, S. Suhai, J. Phys. Chem. B 102, 5899–5913 (1998).
- 26. R. F. Egerton, Ultramicroscopy 180, 115-124 (2017).

#### **ACKNOWLEDGMENTS**

The authors thank R. Egerton at the University of Alberta for helpful discussions regarding the maximum spatial resolution of aloof EELS. The authors also thank A. R. Lupini at ORNL and R. F. Klie at University of Illinois at Chicago for helpful discussions during the conception and execution of the experiments. Funding: This research was supported by the Center for Nanophase Materials Sciences, which is a U.S. Department of Energy (DOE) Office of Science User Facility (J.A.H., J.H., J.J., J.K.K., and J.C.I.); the DOE Office of Science, Basic Energy Sciences, Chemical Sciences, Geosciences, and Biosciences Division (I.P. and

S.J.-P.); and the Neutron Scattering Division (J.K.K.). This research was conducted, in part, using instrumentation within ORNL's Materials Characterization Core provided by UT-Battelle, LLC, under contract no. DE-AC05-000R22725 with the DOE. Theoretical calculations used resources of the National Energy Research Scientific Computing Center, which is supported by the DOE Office of Science under contract no. DE-AC02-05CH11231. Author contributions: J.C.I. developed the experimental concept with input from I.P. and S.J.-P and also advised in the EELS experiments, data analysis, and manuscript preparation. J.A.H. performed the experiments, analyzed the data, prepared

the figures, and wrote the main text of the manuscript. J.H. and J.J. performed the theoretical calculations and advised in the experimental data interpretation. I.P. performed the FTIR experiments. J.K.K. performed XRD measurements and Rietveld refinements. T.C.L., N.D., and O.L.K. developed the 30-kV ultrahigh resolution EELS spectrometer used here and helped with the acquisition of the EELS data at the Nion R&D facility. All authors discussed the results and contributed to the revision of the manuscript. **Competing interests:** T.C.L., N.D., and O.L.K. declare a financial interest in Nion Company. **Data and materials availability:** All data needed to evaluate the

conclusions in the paper are present in the paper or the supplementary materials.

#### SUPPLEMENTARY MATERIALS

www.sciencemag.org/content/363/6426/525/suppl/DC1 Materials and Methods Figs. S1 to S9 References (27–34)

4 October 2018; accepted 28 December 2018 10.1126/science.aav5845



### Identification of site-specific isotopic labels by vibrational spectroscopy in the electron microscope

Jordan A. Hachtel, Jingsong Huang, Ilja Popovs, Santa Jansone-Popova, Jong K. Keum, Jacek Jakowski, Tracy C. Lovejoy, Niklas Dellby, Ondrej L. Krivanek and Juan Carlos Idrobo

Science 363 (6426), 525-528. DOI: 10.1126/science.aav5845

**PERMISSIONS** 

Mapping isotopically labeled alanine

Electron microscopy of organic materials must avoid the destructive effects of electron beam impact. One approach is to measure vibrational spectra with electron energy-loss spectroscopy in a mode where the electron beam mode where the electron beam impact. grazes the sample and couples to it through evanescent modes. Hachtel et al. used such methods to probe carbon-12and carbon-13-labeled alanine crystals, which exhibited an isotopic shift in the asymmetric carbon-oxygen stretching mode. They used this property to map the distribution of labeled clusters of alanine on length scales of tens of nanometers.

Science, this issue p. 525

ARTICLE TOOLS	http://science.sciencemag.org/content/363/6426/525
SUPPLEMENTARY MATERIALS	http://science.sciencemag.org/content/suppl/2019/01/30/363.6426.525.DC1
REFERENCES	This article cites 32 articles, 4 of which you can access for free http://science.sciencemag.org/content/363/6426/525#BIBL

http://www.sciencemag.org/help/reprints-and-permissions

Use of this article is subject to the Terms of Service